

PHOTOPRODUCTION OF THE ISOLATED PHOTON AT HERA IN NLO QCD

M. KRAWCZYK, A. ZEMBRZUSKI

*Institute of Theoretical Physics, Warsaw University, ul. Hoża 69, 00-681 Warsaw, Poland
 E-mail: krawczyk@fuw.edu.pl, azem@fuw.edu.pl*

The NLO QCD calculation for the photoproduction of the isolated photon with a large p_T at the HERA ep collider is presented. The single resolved photon contribution and the QCD corrections of order α_s to the Born term are consistently included. The NNLO contributions, the box and the double resolved photon subprocesses, are sizeable and are taken into account in addition. The importance of the isolation cut, as well as the influence of other experimental cuts on the p_T and η_γ (the final photon rapidity) distributions are discussed in detail. The investigation of the renormalization scale dependence is performed in order to estimate the size of missing higher order QCD corrections. Results are compared with experimental data and with the prediction of a different NLO calculation.

1 Introduction

The production of the prompt photon with large transverse momentum, p_T , in the ep collision is considered. Such reaction is dominated by events with almost real photons mediating the ep interaction, $Q^2 \approx 0$, so in practice we deal with the photoproduction of the prompt photon. The other name for such process is Deep Inelastic Compton (DIC) scattering (although $Q^2 \approx 0$, the scattering is "deep inelastic" due to a large transverse momentum of the final photon). The photon emitted by the electron may interact with the proton partons directly or as a resolved one. Analogously, the observed final photon may arise directly from hard partonic subprocesses or from fragmentation processes, where a quark or a gluon decays into the photon.

The importance of the DIC process in the ep collision for testing the Parton Model and then the Quantum Chromodynamics was studied previously by many authors^{1–9}. Measurements were performed at the HERA ep collider by the ZEUS group^{10–12}, also the H1 Collaboration has presented preliminary results¹³. In these experiments only events with isolated photons were included in the analysis, i.e. with a restriction imposed on the hadronic energy detected close to the photon. The corresponding cross sections for the photoproduction of an isolated photon and of an isolated photon plus jet were calculated in QCD in next-to-leading order (NLO)^{14–17}. There also exists analogous calculation for the large- Q^2 ep collision (DIS events)¹⁸.

In this paper the results of the NLO QCD calculation for the DIC process with an isolated photon at the HERA ep collider are presented. We consider the parton distributions in the photon and parton fragmentation into the photon as quantities of order α_{em} . Our approach differs from the NLO approach^{14–16} by set of subprocesses in-

cluded in the analysis. The comparison of our predictions with the NLO results obtained by L.E. Gordon (LG)¹⁶ is presented for cross sections with kinematical cuts as in the ZEUS Collaboration measurements¹².

The present analysis is the final, much extended and improved version of the previous one¹⁷. We show results for non-isolated final photon, and we study the influence of the isolation cut on the production rate of the photon. The role of other specific cuts applied by the ZEUS Collaboration are discussed and the comparison with data¹² is made. We emphasize the importance of the box diagram $\gamma g \rightarrow \gamma g$, being the higher order process, in description of the data.

We study the renormalization scale dependence of the cross section in order to estimate the size of missing higher order (NNLO or higher) QCD corrections. The NLO results for the photoproduction of the isolated γ are compared to the leading logarithm (LL) ones, and in addition the LL predictions for isolated $\gamma + jet$ final state are presented.

In the recent ZEUS analysis of the prompt photon plus jet production¹⁹ the intrinsic transverse momentum of partons in the proton was included in Monte Carlo simulations to improve agreement between data and predictions. This momentum is not included in our calculations.

We start with discussion on the choice of relevant diagrams defining our NLO approach to the DIC process (sec. 2). The isolation of the photon is described in sec. 3, and the equivalent photon approximation in sec. 4. In secs. 5 and 6 the results of numerical calculations are presented and compared with data¹² and other NLO predictions¹⁶. In sec. 7 we show LL predictions for the photon plus jet production. Finally, sec. 8 summarizes our results.

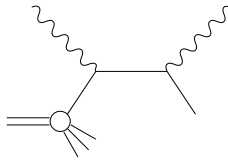


Figure 1: The Born contribution.

2 The NLO calculation for $\gamma p \rightarrow \gamma X$ Deep Inelastic Compton scattering

2.1 General discussion

We start by describing processes which are (should be?) included in the NLO QCD calculations of the cross section for the DIC process,

$$\gamma p \rightarrow \gamma X, \quad (1)$$

where the final photon is produced with large transverse momentum, $p_T \gg \Lambda_{QCD}$. Although we will consider the process (1), the problem which we touch upon is more general - it is related to different approaches to NLO calculations of cross sections for hadronic processes involving resolved photons, see^{6,17} and for more detailed discussion²⁰.

The Born level contribution to the cross section for process (1), i.e. the lowest order in the strong coupling α_s term, arises from the Compton process on the quark (fig. 1):

$$\gamma q \rightarrow \gamma q. \quad (2)$$

It gives the $[\alpha_{em}^2]$ order contributions to the partonic cross section^a. At the same α_{em}^2 order it contributes to the hadronic cross section for the process $\gamma p \rightarrow \gamma X$.

The Parton Model (PM) prediction for the DIC process (1), which applies for $x_T = 2p_T/\sqrt{S} \sim \mathcal{O}(1)$, relies solely on the Born contribution (2)¹, namely:

$$d\sigma^{\gamma p \rightarrow \gamma X} = \sum_q \int dx_p q_p(x_p) d\hat{\sigma}^{\gamma q \rightarrow \gamma q}, \quad (3)$$

where q_p is the quark density in the proton and $d\sigma^{\gamma p \rightarrow \gamma X}$ ($d\hat{\sigma}^{\gamma q \rightarrow \gamma q}$) stands for the hadronic (partonic) cross section. In the QCD improved PM the cross section is given by (3), however with scale dependent quark densities. For semihard processes, where $x_T \ll 1$, the prediction based on the process (2) only is not a sufficient approximation, and one should also consider the contributions corresponding to the collinear showers, involving hadronic-like interactions of the photon(s). There are two classes of such contributions: *single resolved* with resolved initial *or* final photon, and *double resolved* with

^aWe denote the order of partonic subprocesses using square brackets.

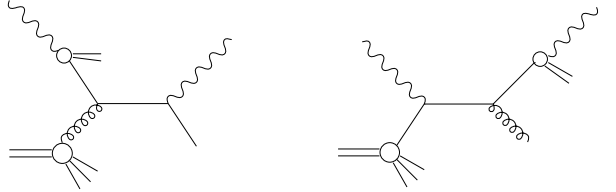


Figure 2: Examples of single resolved processes: a) the resolved initial photon, b) the resolved final photon.

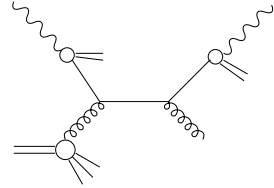


Figure 3: An example of a double resolved photon process.

both the initial *and* the final photon resolved (figs. 2, 3). They correspond to partonic cross sections of orders $[\alpha_{em}\alpha_s]$ (single resolved) and $[\alpha_s^2]$ (double resolved). If one takes into account that partonic densities in the photon and the parton fragmentation into the photon are of order $\sim \alpha_{em}$, then the contributions to the hadronic cross section from these resolved photon processes are $\alpha_{em}^2\alpha_s$ and $\alpha_{em}^2\alpha_s^2$, respectively. Both single and double resolved contributions are included in the standard LL QCD analyses of the DIC process^{4,5,9}.

To obtain the NLO QCD predictions for the process (1) the α_s corrections to the lowest order process (2) have to be calculated leading to terms of order $\alpha_{em}^2\alpha_s$ ^{4,5,21,22} (fig. 4). In these $\alpha_{em}^2\alpha_s$ contributions there are collinear singularities to be subtracted and shifted into corresponding quark densities or fragmentation functions. This way the single resolved photon contribution appears in the calculation of the α_s corrections to the Born process. It is worth noticing that in the NLO expression for the cross section there are no collinear singularities which would lead to the double resolved photon contributions. It indicates that taking into account $[\alpha_s^2]$ subprocesses, associated with both the initial and final photons resolved, goes beyond the accuracy of the NLO calculation. This will be consistent within the

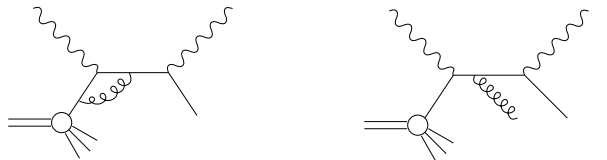


Figure 4: Examples of the virtual gluon and real gluon α_s corrections to the Born contribution.

NNLO approach, where α_s^2 correction to the Born term and α_s correction to the single resolved terms should be included, all giving the same $\alpha_{em}^2 \alpha_s^2$ order contribution to the hadronic cross sections.

The other set of diagrams is considered by some authors^{14–16} in the NLO approach to DIC process (1), due to their different way of counting the order of parton densities in the photon (and the parton fragmentation into the photon). This approach, which we will call “ $1/\alpha_s$ ” approach, is motivated by large logarithms of Q^2 in the F_2^γ existing already in the PM. By expressing $\ln(Q^2/\Lambda_{QCD}^2)$ as $\sim 1/\alpha_s$ one treats the parton densities in photon as proportional to α_{em}/α_s (see e.g.^{3–5,8,9,14–16}). By applying this method to the DIC process, we see that the single resolved photon contribution to the hadronic cross section for $\gamma p \rightarrow \gamma X$ becomes of the same order as the Born term, namely

$$\frac{\alpha_{em}}{\alpha_s} \otimes [\alpha_{em} \alpha_s] \otimes 1 = \alpha_{em}^2. \quad (4)$$

The same is also observed for the double resolved photon contribution

$$\frac{\alpha_{em}}{\alpha_s} \otimes [\alpha_s^2] \otimes \frac{\alpha_{em}}{\alpha_s} = \alpha_{em}^2. \quad (5)$$

We see that by such counting, the same α_{em}^2 order contributions to the hadronic cross section are given by the direct Born process, single and double resolved photon processes although they correspond to quite different final states (observe a lack of the remnant of the photon in the direct process). Moreover, they constitute the lowest order (in the strong coupling constant) term in the perturbative expansion, actually the zeroth order, so the direct dependence of the cross section on the strong coupling constant is absent. If one takes into account that some of these terms correspond to the hard processes involving gluons, the lack of terms proportional to α_s coupling in the cross section seems to be contrary to intuition.

In the “ $1/\alpha_s$ ” approach beside the α_s correction to the Born cross section, the α_s corrections to the single and to the double resolved photon contributions are included in the NLO calculation, since all of them give terms of the same order, $\alpha_{em}^2 \alpha_s$ ^{14–16}.

To summarize, the first approach starts with one basic, direct subprocess as in the PM (eq. 2), while the second one with three different types of subprocesses (as in the standard LL calculation). Obviously, some of NNLO terms in the first method belong to the NLO terms in the second one.

In this paper we apply the first type of NLO approach to the DIC process, however with some important NNLO terms additionally included. A comparison between our results and the results based on the other approach^{14–16} is discussed in sec. 6.3.

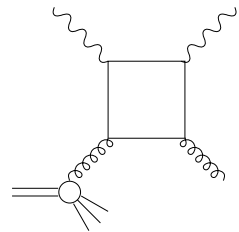


Figure 5: The box diagram.

2.2 The cross section

Below we describe our approach to the DIC process, where the parton densities in the photon and the parton fragmentation into the photon are treated as $\sim \alpha_{em}$.

In the NLO QCD calculation of the DIC process we take into account the following subprocesses:

- the Born contribution (2) (fig. 1);
- the finite α_s corrections to the Born diagram (so called K-term) from virtual gluon exchange, real gluon emission (fig. 4), and the process $\gamma g \rightarrow q\bar{q}\gamma$;
- two types of single resolved photon contributions, with resolved initial and final photons (fig. 2).

Besides the above full NLO set, we will include two terms of order $\alpha_{em}^2 \alpha_s^2$ (formally from the NNLO set): the double resolved contributions (fig. 3) and the direct diagram (box) $\gamma g \rightarrow \gamma g$ ²³ (fig. 5), since they were found to be large^{3–8}.

The cross section for the $\gamma p \rightarrow \gamma X$ scattering has the following form:

$$\begin{aligned} E_\gamma \frac{d^3 \sigma^{\gamma p \rightarrow \gamma X}}{d^3 p_\gamma} = & \sum_b \int dx f_{b/p}(x, \bar{Q}^2) \frac{\alpha_s(\bar{Q}^2)}{2\pi^2 \hat{s}} K_b + \\ & + \sum_{abc} \int \frac{dz}{z^2} \int dx_\gamma \int dx f_{a/\gamma}(x_\gamma, \bar{Q}^2) f_{b/p}(x, \bar{Q}^2) \cdot \\ & \cdot D_{\gamma/c}(z, \bar{Q}^2) E_\gamma \frac{d^3 \sigma^{ab \rightarrow cd}}{d^3 p_\gamma} \end{aligned} \quad (6)$$

The first term is the K-term describing the finite α_s corrections to the Born process, and the second one stands for the sum over all other contributions (including the Born contribution). The $f_{a/\gamma}$ ($f_{b/p}$) is a a (b)-parton distribution in the photon (proton) while the $D_{\gamma/c}$ is a c -parton fragmentation function. For the direct initial (final) photon, where $a = \gamma$ ($c = \gamma$), we take $f_{a/\gamma} = \delta(x_\gamma - 1)$ ($D_{\gamma/c} = \delta(z - 1)$) (the Born contribution is obtained for $a = \gamma$, $b = q$ and $c = \gamma$). The variables x_γ , x and z stand for the fraction of the initial photon, proton, and c -parton momenta taken by the a -parton, b -parton, and the final photon, respectively. The renormalization scale is assumed equal to the factorization scale and is denoted as \bar{Q} .

3 The isolation

In order to observe photons originating from a hard subprocess one should reduce backgrounds, mainly from π^0 's and γ 's radiated from final state hadrons. To achieve this, isolation cuts on the observed photon are introduced in experimental analyses. The isolation cuts are defined by demanding that the sum of hadronic energy within a cone of radius R around the final photon, where the radius R is defined in the rapidity and azimuthal angle space (see eq. 13 in Appendix), should be smaller than the final photon energy multiplied by a small parameter ϵ :

$$\sum_{\text{hadrons}} E_h < \epsilon E_\gamma. \quad (7)$$

The simplest way to calculate the differential cross section for an isolated photon, $d\sigma_{\text{isol}}$, is to calculate the difference of a non-isolated differential cross section, $d\sigma_{\text{non-isol}}$, and a subtraction term, $d\sigma_{\text{sub}}$ ^{24–26,14}:

$$d\sigma_{\text{isol}} = d\sigma_{\text{non-isol}} - d\sigma_{\text{sub}}. \quad (8)$$

The subtraction term corresponds to cuts opposite to the isolation cuts, i.e. hadrons with the total energy higher than the photon energy multiplied by ϵ should appear within a cone of radius R around the final photon.

The isolation cuts are imposed only when calculating the K-term, and in contributions involving fragmentation function (resolved final photon). Other contributions arise from $2 \rightarrow 2$ subprocesses with direct final photon that is isolated by definition.

In the analysis we apply the subtraction method with the subtraction term calculated in an approximate way, see^{25,14} for details. The approximation bases on the assumption that an angle δ between the final photon and a parton inside the cone of radius R is small. It allows to simplify considerably the calculations and leads to compact analytical expressions for all relevant matrix elements involved in $d\sigma_{\text{sub}}$. Note that in this approximation the angle δ is simply proportional to the radius R : $\delta = R/\cosh(\eta_\gamma)$. The above small- δ approximation is used only in calculation of the K -term in the subtraction cross section $d\sigma_{\text{sub}}$, for the results see Appendix. Other contributions to $d\sigma_{\text{sub}}$, as well as $d\sigma_{\text{non-isol}}$ and all LL expressions, are obtained in an exact way.

It is worth mentioning that there is an ongoing discussion whether the conventional factorization breaks down, and whether the cross section is an infrared safe quantity for isolated photon photoproduction in e^+e^- collisions (also for hadron-hadron reactions)^{27,28}. In principle these questions could as well occur for the photoproduction of isolated photons in ep collisions. However we do not deal with this problem because it arises

from $2 \rightarrow 3$ subprocesses in which a final quark fragments into a photon. We checked this explicitly and found that all singularities in $d\sigma_{\text{sub}}$ are canceled or factorized, as in $d\sigma_{\text{non-isol}}$. Therefore the considered by us cross section $d\sigma_{\text{isol}}$ is well defined (see also^{14,16,18}).

4 The equivalent photon approximation

We consider the production of photons with large transverse momentum, $p_T \gg \Lambda_{QCD}$, in the ep scattering, $ep \rightarrow e\gamma X$, at the HERA collider. This reaction is dominated by photoproduction events, i.e. the electron is scattered at a small angle and the mediating photon is almost real, $Q^2 \approx 0$. The cross section for such processes can be calculated using the equivalent photon (Williams-Weizsäcker) approximation²⁹ which relates the differential cross section for ep collision to the differential cross section for γp collision. For the DIC scattering the approximation has the following form:

$$d\sigma^{ep \rightarrow e\gamma X} = \int G_{\gamma/e}(y) d\sigma^{\gamma p \rightarrow \gamma X} dy, \quad (9)$$

where y is (in the laboratory frame) a fraction of the initial electron energy taken by the photon.

We apply the equivalent photon approximation and take the (real) photon distribution in the electron in the form³⁰:

$$G_{\gamma/e}(y) = \frac{\alpha_{em}}{2\pi} \left\{ \frac{1 + (1 - y)^2}{y} \ln \left[\frac{Q_{\text{max}}^2(1 - y)}{m_e^2 y^2} \right] - \frac{2}{y} \left(1 - y - \frac{m_e^2 y^2}{Q_{\text{max}}^2} \right) \right\}, \quad (10)$$

with m_e being the electron mass. In the numerical calculations we assume Q_{max}^2 as 1 GeV² what is a typical value for the recent photoproduction measurements at the HERA collider.

5 The results and comparison with data

The results for the non-isolated and isolated photon cross sections are obtained in NLO accuracy with additional NNLO terms, as discussed in sec. 2.2. We take the HERA collider energies: $E_e = 27.5$ GeV and $E_p = 820$ GeV¹², and we consider the p_T range of the final photon between 5 and 20 GeV (x_T from 0.03 to 0.13). The calculations are performed in $\overline{\text{MS}}$ scheme with a hard (renormalization, factorization) scale \bar{Q} equal p_T . Also $\bar{Q} = p_T/2$ and $2p_T$ are used to study the dependence of the results on the choice of \bar{Q} . We neglect the quark masses and assume the number of active flavors to be $N_f = 4$ (and for comparison also $N_f = 3$ and 5). The two-loop coupling constant α_s is

used in the form

$$\alpha_s(\bar{Q}^2) = \frac{4\pi}{\beta_0 \ln(\bar{Q}^2/\Lambda_{QCD}^2)} \left[1 - \frac{2\beta_1}{\beta_0^2} \frac{\ln[\ln(\bar{Q}^2/\Lambda_{QCD}^2)]}{\ln(\bar{Q}^2/\Lambda_{QCD}^2)} \right] \quad (11)$$

($\beta_0 = 11 - 2/3N_f$ and $\beta_1 = 51 - 19/3N_f$), with $\Lambda_{QCD}=0.365, 0.320$ and 0.220 GeV for $N_f=3, 4$ and 5 , respectively, as fitted by us to the experimental value of $\alpha_s(M_Z) = 0.1177^{31}$. The $\Lambda_{QCD}^{LL} = 0.120$ GeV for $N_f=4$ was taken in one-loop α_s when calculating the cross section in LL accuracy.

We use the GRV parametrizations of the proton structure function (NLO and LO)³², the photon structure function (NLO and LO)³³, and the fragmentation function (NLO)³⁴. For comparison other parametrizations are also used: DO⁴, ACFGP⁸, CTEQ³⁵, MRST³⁶ and GS³⁷.

As the reference we take the GRV NLO set of parton distributions^{32–34}, $N_f = 4$, $\Lambda_{QCD} = 320$ GeV and $\bar{Q} = p_T$.

5.1 Non-isolated versus isolated photon cross section

The p_T distribution for the produced final photon without any cut is presented in fig. 6 where the NLO results and separately the Born term (with NLO parton densities) are shown. The cross section decreases by three orders of magnitude when p_T increases from 4 GeV to 20 GeV, and obviously the most important contribution is coming from the lowest p_T region. The subprocesses other than the Born one give all together contribution almost two times larger than the cross section for the Born subprocess alone.

The importance of particular contributions to the non-isolated cross section integrated over $5 \text{ GeV} < p_T < 10 \text{ GeV}$ is illustrated in Table 1 (the first line). The total NLO cross section is equal to 226 pb, with individual contributions equal to: *Born* = 36.3%, *single resolved* = 35.1%, *double resolved* = 18.7%, *box* = 6.2%, *K-term* = 3.9%. We see that the single resolved photon processes give a contribution comparable to the Born term. Also the double resolved photon processes are important. It is worth noticing that the overall double resolved photon cross section is build from many, relatively small, individual terms. The direct box diagram ($\gamma g \rightarrow \gamma g$) gives 17% of the Born ($\gamma q \rightarrow \gamma q$) contribution. Relatively large box contribution (although being $[\alpha_s^2]$) is such partially due to large gluonic content of the proton at small x_p .

Next, in fig. 7 we compare the differential cross section $d\sigma/d\eta_\gamma$ for the non-isolated photon with corresponding predictions for the isolated photon using various values of the isolated cone variables (ϵ, R)^b. The isolat-

tion cut suppresses the cross section by above 10% in the whole rapidity range. For $\epsilon=0.1$ and $R = 1$ the suppression is 17-23% at rapidities $-1.5 < \eta_\gamma \leq 4$. This large effect is not too sensitive to the value of ϵ : changing the value by a factor of 2 from $\epsilon = 0.1$ to $\epsilon = 0.2$ or to $\epsilon = 0.05$ varies the results for isolated photon by about 4% (fig. 7a). The dependence on R is stronger but also not very large: when changing R value by a factor of 2 from 1 to 0.5 the results increase by about 7% (fig. 7b).

The suppression due to the isolation imposed on the photon is presented in Table 1 (the second line) for individual contributions and for the total cross section. As expected, the cross section for fragmentation processes (i.e. with resolved final photon) is strongly suppressed: after isolation it is lowered by a factor of 5. At the same time the QCD corrections to the Born diagram increase significantly, i.e. the contribution to the subtraction cross section, $d\sigma_{sub}$, due to this corrections is negative. The isolation restrictions do not modify contributions of other subprocesses since they involve photons isolated by definition. The subtraction cross section, being a sum of negative QCD corrections and fragmentation contributions, is of course positive and the total cross section for isolated final photon is lower, by 20%, than for the non-isolated one.

In the following we keep $R=1$ and $\epsilon=0.1$, standard values used in both theoretical and experimental analyses.

5.2 Other experimental cuts

In order to compare the results with data we consider other cuts imposed by the ZEUS group on prompt photon events at the HERA collider¹². The influence of the limited energy range, $0.2 \leq y \leq 0.9$, is shown in fig. 8. The cross section is strongly reduced, by 30-85%, in the positive rapidity region. At negative rapidities the change due to the y -cut is weaker: 5-10% at $-1.2 < \eta_\gamma \leq -0.4$ and 10-30% at other negative rapidities. Separately we show the results obtained without the box subprocess (fig. 8). The box diagram contributes mainly in the rapidity region between -1 and 3. After imposing the y -cut its contribution is important in narrower region from -1 to 1. The influence of the y -cut can be read also from Table 1 (the third line). One sees e.g. that the Born contribution is reduced 3.5 times, while other ones are suppressed less, roughly by a factor of 2.

The results obtained for the isolated photon with the y -cut and in addition with the cut on the final photon rapidity, $-0.7 \leq \eta_\gamma \leq 0.9$, are presented in the last line of Table 1. The restriction on η_γ decreases the contributions of all subprocesses approximately by a factor of 2 (except for the double resolved contribution reduced almost 3 times).

^bThe positive rapidity is pointed in the proton direction.

The role of various experimental cuts is illustrated also in fig. 9, this time for the x_γ distribution. In particular we see that the isolation and the energy cut reduce considerably the contributions from large and medium x_γ , while the contributions from x_γ below 0.1 are reduced less. On the other hand, the small x_γ contributions are strongly, by two orders of magnitude, diminished by the photon rapidity cut. This shows that measurements at the central η^γ region ($-0.7 \leq \eta^\gamma \leq 0.9$) are not too sensitive to the small x_γ values in the photon.

When calculating the QCD corrections to the Born process in the subtraction term $d\sigma_{sub}$ we used the small- δ approximation described in sec. 3. Because these corrections give less than 10% of the cross section for the isolated photon production with various cuts (see the third column in Table 1), we expect that the error resulting from using the approximations is small, though we use in fact not a small value of δ ($\delta = R/\cosh\eta_\gamma$, $R = 1$).^c

5.3 The comparison with data

Two types of the final state were measured in the ZEUS experiment: 1) an isolated photon with $-0.7 \leq \eta^\gamma \leq 0.9$ and $5 \leq p_T \leq 10$ GeV; 2) an isolated photon plus jet with the photon rapidity and transverse momentum as above, the jet rapidity in the range $-1.5 \leq \eta^{jet} \leq 1.8$, and the jet transverse momentum $p_T^{jet} \geq 5$ GeV.

We compare our NLO predictions with the ZEUS data from the first type of measurements¹². In fig. 10a the comparison is made for the transverse momentum distribution for various N_f . Although the predictions tend to lie slightly below the data a satisfactory agreement is obtained for $N_f = 4$. Note a large difference between the results for $N_f=4$ and 3 due to the fourth power of electric charge characterizing processes with two photons. We observe a very small contribution from the bottom quark (for $N_f=5$). The predictions are obtained in massless quark scheme and may overestimate the production rate.

Similar comparison of the NLO results with the data, now for the rapidity distribution, is shown in fig. 10b. A good description of the data is obtained for $N_f=4$ and $N_f=5$ in the rapidity region $0.1 \leq \eta_\gamma \leq 0.9$. For $-0.7 \leq \eta_\gamma \leq 0.1$ our predictions lie mostly below the experimental points. This disagreement between predicted and measured cross sections is observed also for other theoretical calculations (LG) and for Monte Carlo sim-

^cCalculations for the prompt photon production in ep ¹⁶ and hadron-hadron³⁸ collisions were performed using space slicing method without the small δ assumption. Comparison of such results with predictions obtained in (discussed here) approximated way showed that the small δ approximation is an accurate analytic technique for including isolation effects in NLO calculations (also for $R = 1$)¹⁶.

ulations¹²^d. In fig. 10b we present separately an effect due to the box subprocess (for $N_f = 4$). It is clear that the box term enhances considerably the cross section in the measured rapidity region. Its contribution to the integrated cross section is equal to 9.6%. The double resolved photon contribution is also sizeable, although roughly two times smaller than the box one, see Table 1 (fourth line). Both these $[\alpha_s^2]$ contributions improve description of the data.

The predictions obtained using three different NLO parton densities in the photon (ACFGP⁸, GRV³³ and GS³⁷) are presented for $N_f = 4$ in fig. 11a ($\bar{Q} = p_T$) and in fig. 11b ($\bar{Q} = 2p_T$) together with the ZEUS data¹². The results based on ACFGP and GRV parametrizations differ by less than 4% at rapidities $\eta_\gamma < 1$ (at higher η_γ the difference is bigger), and both give good description of the data in the rapidity range $0.1 \leq \eta_\gamma \leq 0.9$ (for $\bar{Q} = p_T$ and $\bar{Q} = 2p_T$). For $-0.7 \leq \eta_\gamma \leq 0.1$ none of the predictions is in agreement with the measured cross section.

For $\bar{Q}=p_T$ (fig. 11a) the GS distribution leads to results considerably below ones obtained using ACFGP and GRV densities, especially in the rapidity region from roughly -1 to 1. This difference between the GS and other considered herein parton parametrizations is mainly due to their different treatment of the charm quark in the photon. In the GS approach the charm quark is absent for \bar{Q}^2 below 50 GeV². Since we take $5 \leq \bar{Q} = p_T \leq 10$ GeV, and the most important contribution to the cross section arises from the lower p_T region (see fig. 10a), the \bar{Q}^2 value usually lies below the GS charm quark threshold. As a consequence, predictions based on GS have strongly suppressed the contribution of subprocesses involving charm from the photon - contrary to GRV and ACFGP predictions where the charm threshold is at lower \bar{Q}^2 .

The above explanation of differences between cross sections involving GS and both GRV and ACFGP parton densities is insufficient for higher rapidities, $\eta_\gamma > 2$. Here the differences between the results based on particular photon parametrizations are bigger, especially when comparing predictions obtained using GRV and ACFGP ones (not shown). This is due to large differences between used parton densities at low x_γ , which is probed at the high rapidity region.

All the considered parton distributions give similar description of the data when the scale is changed to

^dThe ZEUS Collaboration has presented recently an analysis¹⁹ in which an intrinsic transverse momentum of partons in the proton, k_T , was introduced in the PYTHIA 6.1 generator in order to improve agreement between the data and Monte Carlo predictions for an isolated photon plus jet photoproduction. The data, selected with $x_\gamma > 0.9$, are consistent with the predictions for $\langle k_T \rangle = 1.69 \pm 0.18^{+0.18}_{-0.20}$ GeV.

$\bar{Q} = 2p_T$, see fig. 11b. Here the calculation corresponds to \bar{Q}^2 which is always above 50 GeV^2 and the charm density in the GS parametrization is non-zero, as in other parametrizations.

In fig. 12 our predictions are compared to the ZEUS data divided into three ranges of y . This allows to establish that the above discussed discrepancy between the data and the predictions for $\eta^\gamma < 0.1$ is coming mainly from the low y region, $0.2 < y < 0.32$. In the high y region, $0.5 < y < 0.9$, a good agreement is obtained.

We have also studied the dependence of our results on the choice of the parton distributions in the proton and parton fragmentation into the photon (not shown). Cross sections calculated using GRV³², MRST (set ft08a)³⁶ and CTEQ4M³⁵ NLO parton parametrizations for the proton vary among one another by 4 to 7% at negative rapidities and less than 4% at positive rapidity values. Results for the isolated final photon are also not too sensitive to the fragmentation function. For rapidity ranging from -1 to 4 the cross section obtained with DO LO⁴ fragmentation function is 2 – 3.5% lower than the cross section based on GRV NLO³⁴ parametrization. Only at minimal ($\eta_\gamma < -1$) and maximal ($4 < \eta_\gamma$) rapidity values this difference is larger, being at a level of 3.5 – 8%.

6 The theoretical uncertainties of the results and comparison with other NLO predictions

As we already mentioned the predictions are obtained in massless quark scheme and may overestimate the production rate. An improved treatment of the charm quark, especially in the box contribution which is particularly sensitive to the change from $N_f = 3$ to $N_f = 4$, would be needed. However we do not expect that this improvement would change qualitatively our results.

We now discuss the theoretical uncertainties of our predictions related to the perturbative expansion.

6.1 The dependence on the \bar{Q} scale

In order to estimate the contribution due to missing higher order terms, the influence of the choice of the \bar{Q} scale is studied for the η_γ distribution. In fig. 13a the results obtained using GRV densities with and without the y -cut are shown. When changing \bar{Q} from p_T to $2p_T$ ($p_T/2$) the cross section increases (decreases) at rapidities below ~ 1 and decreases (increases) at higher rapidity values. Only at high rapidities (where the cross section is small), $\eta_\gamma > 3$, the dependence on the choice of the scale is strong, above 10% (up to 20-30% at $\eta_\gamma \approx 5$). In the wide kinematical region, $-2 < \eta_\gamma < 2$, the relative differences between results (with and without the y -cut) for $\bar{Q} = p_T$ and results for $\bar{Q} = 2p_T$ or $p_T/2$ are

small and do not exceed 6%. Around the maximum of the cross section at rapidities $-1 \leq \eta_\gamma \leq 0$ these differences are 4-6%. This small sensitivity of the results to the change of the scale is important since it indicates that the contribution from neglected NNLO and higher order terms is not significant.

Note that individual contributions are strongly dependent on the choice of \bar{Q} , e.g. results for the single resolved processes vary by $\pm 10\text{--}20\%$ at rapidities $\eta_\gamma \leq 1$. Results are much more stable only when the sum of resolved processes and QCD corrections is considered.

In fig. 13b we present NLO results for various \bar{Q} with and without the y -cut, however this time with no box contribution. At rapidities $\eta_\gamma < 1$ the uncertainty due to the choice of the renormalization scale is about two times higher than for the cross section with included box diagram, so the box contribution ($\sim [\alpha_s^2]$) seems to stabilize the NLO prediction. At rapidities $\eta_\gamma > 2$ the relative dependence on the choice of the scale is similar for the cross section with and without the box term.

6.2 The comparison of NLO and LL predictions

In the present calculation we include in LL accuracy the single and double resolved photon processes as well as the box diagram in addition to the Born contribution, see also^{3–5,9} (although this is not fully consistent with the discussion in sec. 2). The cross section for the $\gamma p \rightarrow \gamma X$ scattering in LL accuracy is obtained by convolution of partonic cross sections with relevant LO parton densities.

In fig. 14 we show the LL prediction for the isolated γ photoproduction (dotted line) together with NLO predictions (solid line) and the Born contribution only (dot-dashed line). The highest differences between the LL and NLO cross sections are seen at the rapidity range $-0.5 < \eta_\gamma < 2.5$ where the LL results lie 10-20% below the NLO ones (fig. 14a). For the p_T distribution this difference is 10-14% in the whole presented range of the transverse momentum, $4 \leq p_T \leq 20 \text{ GeV}$ (fig. 14b).

We think that the observed difference between NLO and LL results together with the weak dependence on the \bar{Q} scale discussed in sec. 6.1 indicates reliability of the calculation.

6.3 The comparison with other NLO results

As we discussed in Sec. 2, our NLO calculation of the DIC process differs from the “ $1/\alpha_s$ ”-type NLO analysis presented in ref.^{14–16}, by set of diagrams included in the calculation. We do not take into account α_s corrections to the single and double resolved processes, which are beyond the NLO accuracy in our approach. On the other hand, we include the box diagram neglected in^{14–16}.

(The double resolved subprocesses are included in both analyses.)

We compare our results and the results of the LG calculation¹⁶ (using $N_f=4$ and $\bar{Q} = p_T$) for the isolated final photon ($R=1$, $\epsilon=0.1$) in the kinematical range as in the ZEUS analysis¹² (i.e. for $-0.7 \leq \eta^\gamma \leq 0.9$ and $0.2 \leq y \leq 0.9$). First we use the GRV photon parton densities. The LG predictions for $d\sigma/dp_T$ cross section are about 20% higher than ours in the presented range of transverse momentum, $4 \leq p_T \leq 20$ GeV. For $d\sigma/d\eta^\gamma$ cross section (with $5 \leq p_T \leq 10$ GeV) the biggest differences are at $\eta^\gamma=0.9$ where the LG results are about 35% higher. The differences decrease towards negative rapidity values and are negligible at $-0.7 \leq \eta^\gamma < -0.5$. For y range limited to low values only, $0.2 < y < 0.32$, the LG cross section is higher than ours by up to 20% at positive η_γ , while at negative η_γ it is lower by up to 10%. For large y values, $0.5 < y < 0.9$, where our predictions agree with data, the LG results are higher than ours by up to 80% (at $\eta_\gamma = 0.9$).

As it was already discussed, for $\bar{Q} = p_T$ the GS photon distributions lead to results lower by 11-14% than those obtained with GRV densities at rapidities between -1 and 1 (see sec. 5.3). In calculations presented in¹⁴⁻¹⁶ this difference is even twice larger.

The LG predictions¹⁶ obtained using the GS parametrization lie up to 20% below ours (also based on GS distributions, with $\bar{Q} = p_T$ and $N_f = 4$) at rapidities $-0.7 \leq \eta_\gamma \leq 0.2$, and they are higher than ours by up to 30% for $0.2 \leq \eta_\gamma \leq 0.9$ ^{16,12}.

7 The LL prediction for $\gamma + jet$ photoproduction

The ZEUS Collaboration has also analyzed the prompt photon photoproduction in which in addition a hadron jet is measured^{10,11,19}. In fig. 14 we show the LL prediction for the isolated $\gamma + jet$ final state^e together with the predictions for the γ alone. The following jet rapidity and transverse momentum are assumed: $-1.5 \leq \eta_{jet} \leq 1.8$ and $p_T^{jet} > 5$ GeV, respectively. This additional cuts for the final state imposed on jets decrease the cross section, especially at high rapidities. The LL predictions for the $\gamma + jet$ are lower than those for the γ production by 5-10% at negative rapidities and by 10-80% at positive rapidity values. The difference between both LL results is about 10% in wide range of transverse momenta, $\sim 6 \leq p_T \leq 20$ GeV, and only for the lower p_T region, $4 \leq p_T \leq 6$ GeV, it is higher (13-23%).

^eThe NLO calculation for $\gamma + jet$ photoproduction will be discussed in our next paper.

8 Summary

Results of the NLO calculation, with NNLO contributions from double resolved photon processes and box diagram, for the isolated γ production in the DIC process at HERA are presented^f. The role of the kinematical cuts used in the ZEUS measurement¹² are studied in detail.

The results obtained using GRV parametrizations agree with the data in shape and normalization for p_T distribution. For η^γ distribution a good description of the data is obtained for $\eta^\gamma > 0.1$, while for $\eta^\gamma < 0.1$ the data usually lie above the predictions. This discrepancy arises mainly from the low y region, $0.2 \leq y \leq 0.32$. The beyond NLO terms, especially a box contribution, improve the description of the data.

We have studied the theoretical uncertainty of results due to the choice of the renormalization/factorization scale: $\bar{Q} = p_T/2, p_T, 2p_T$. At high rapidities $\eta_\gamma > 3$, where the cross section is small, the uncertainty is 10-30%. In a wide range of rapidities, $-2 \leq \eta_\gamma \leq 2$, the dependence on the \bar{Q} scale is small, below 6%. Since we include some NNLO diagrams in our NLO calculation, this stability of the predictions versus the change of the scale is especially important. The weak dependence on the \bar{Q} scale, and not large differences between LL and NLO predictions (below 20%) allows to conclude that theoretical uncertainties of our NLO calculations for an isolated photon production in the DIC process at HERA are relatively small.

We compared our results with the LG ones based on different set of subprocesses. The cross section $d\sigma/dp_T$ obtained by LG is about 20% higher than ours (for GRV photonic parton distributions). For the cross section $d\sigma/d\eta_\gamma$ this difference is up to 35% at $\eta_\gamma = 0.9$. The highest differences are present for high y values only, $0.5 < y < 0.9$, where on the other hand our predictions are in agreement with the data. At low y range, $0.2 < y < 0.32$, differences between both calculations are smaller and none of them describe the data well for rapidities below 0.1.

Acknowledgements

We would like to acknowledge P. Bussey, Sung W. Lee and L.E. Gordon for important discussions.

Supported in part by Polish State Committee for Scientific Research, grants number 2P03B18410 (1998-1999), 2P03B11414 (2000) and 2P03B05119 (2000-2001), by Interdisciplinary Centre for Mathematical and Computational Modelling, Warsaw University, Grant No G16-10

^fOur fortran code is available upon request from azem@fuw.edu.pl.

(1999-2000), and by European Commission 50th framework contract HPRN-CT-2000-00149.

References

1. J. D. Bjorken and E. A. Paschos, Phys. Rev. **185** (1969) 1975
2. T. Tu, C. Wu, Nucl. Phys. B **156** (1979) 493
3. M. Fontannaz and D. Schiff, Z. Phys. C **14** (1982) 151
4. D. W. Duke and J. F. Owens, Phys. Rev. D **26** (1982) 1600; Err: Phys. Rev. D **28** (1983) 1227
5. P. Aurenche, A. Douiri, R. Baier, M. Fontannaz and D. Schiff, Z. Phys. C **24** (1984) 309
6. M. Krawczyk, Acta Physica Polonica B **21** (1990) 999
7. A. C. Bawa, M. Krawczyk and W. J. Stirling, Z. Phys. C **50** (1991) 293;
A. C. Bawa and M. Krawczyk, Phys. Lett. B **262** (1991) 492;
A. C. Bawa and M. Krawczyk, Proc. "Physics at HERA", Hamburg 1991, p. 579, IFT-17-91;
M. Krawczyk, IFT-17-92, *Talk given at 27th Rencontres de Moriond: QCD and High Energy Hadronic Interactions, Les Arcs, France, 1992*
8. P. Aurenche, P. Chiappetta, M. Fontannaz, J. P. Guillet and E. Pilon, Z. Phys. C **56** (1992) 589
9. L. E. Gordon and J. K. Storrow, Z. Phys. C **63** (1994) 581
10. ZEUS Coll., J. Breitweg et al., Phys. Lett. B **413** (1997) 201
11. ZEUS Coll., *Subm. to the XXIXth International Conference on High-Energy Physics (ICHEP 98), Vancouver, Canada, 1998, abstract 815*
12. ZEUS Coll., J. Breitweg et al., Phys. Lett. B **472** (2000) 175
13. H1 Coll., *Subm. to the International Europhysics Conference on High Energy Physics, HEP97, Jerusalem, Israel, 1997, abstract 265*
14. L. E. Gordon and W. Vogelsang, Phys. Rev. D **52** (1995) 58
15. L. E. Gordon and W. Vogelsang, hep-ph/9606457, *Talk presented by W. Vogelsang at the Int. Workshop on Deep Inelastic Scattering and Related Phenomena, Rome, Italy, 1996*
16. L. E. Gordon, Phys. Rev. D **57** (1998) 235
17. M. Krawczyk and A. Zembrzuski, hep-ph/9810253, IFT 98/12, *Contribution to the XXIXth International Conference on High Energy Physics, ICHEP'98, Vancouver, Canada, 1998, abstract 889*
18. G. Kramer, D. Michelisen and H. Spiesberger, Eur. Phys. J. C **5** (1998) 293;
A. Gehrmann-De Ridder, G. Kramer and H. Spiesberger, Phys. Lett. B **459** (1999) 271; Eur. Phys. J. C **11** (1999) 137; Nucl. Phys. B **578** (2000) 326
19. [ZEUS Collaboration], hep-ex/0104001.
20. J. Chýla, JHEP 0004 (2000) 007; hep-ph/9811455; hep-ph/0010140; hep-ph/0010309
21. M. Krawczyk, unpublished
22. J. Źochowski, "The corrections of order α_S in Deep Inelastic Compton Scattering", *MS Thesis, 1992*
23. B. L. Combridge, Nucl. Phys. B **174** (1980) 243
24. E. L. Berger and J. Qiu, Phys. Lett. B **248** (1990) 371; E. L. Berger and J. Qiu, Phys. Rev. D **44** (1991) 2002
25. L. E. Gordon and W. Vogelsang, Phys. Rev. D **50** (1994) 1901
26. M. Glück, L. E. Gordon, E. Reya and W. Vogelsang, Phys. Rev. Lett. **73** (1994) 388
27. E. L. Berger, X. Guo and J. Qiu, Phys. Rev. Lett. **76** (1996) 2234; Phys. Rev. D **54** (1996) 5470; hep-ph/9610497; hep-ph/9708408
28. P. Aurenche, M. Fontannaz, J. P. Guillet, A. Kotikov and E. Pilon, Phys. Rev. D **55** (1997) R1124;
S. Catani, M. Fontannaz and E. Pilon, Phys. Rev. D **58** (1998) 094025
29. C. F. von Weizsäcker, Z. Phys. **88** (1934) 612;
E. J. Williams, Phys. Rev. **45** (1934) 729; E.J. Williams, Kgl. Danske Vidensk. Selskab. Mat.-Fiz. Medd. 13 (1935) N4
30. V. M. Budnev, I. F. Ginzburg, G. V. Meledin and V. G. Serbo, Phys. Rep. **15** (1975) 181;
R. Nisius, Phys. Rep. **332** (2000) 165
31. O. Biebel, P. A. Movilla Fernandez, S. Bethke and the JADE Coll., Phys. Lett. B **459** (1999) 326
32. M. Glück, E. Reya and A. Vogt, Z. Phys. C **67** (1995) 433
33. M. Glück, E. Reya and A. Vogt, Phys. Rev. D **45** (1992) 3986; M. Glück, E. Reya and A. Vogt, Phys. Rev. D **46** (1992) 1973
34. M. Glück, E. Reya and A. Vogt, Phys. Rev. D **48** (1993) 116
35. H.L. Lai, J. Huston, S. Kuhlmann, F. Olness, J. Owens, D. Soper, W.K. Tung, and H. Weerts, Phys. Rev. D **55** (1997) 1280
36. A. D. Martin, R. G. Roberts, W. J. Stirling and R. S. Thorne, Eur. Phys. J. C **4** (1998) 463
37. L. E. Gordon and J. K. Storrow, Nucl. Phys. B **489** (1997) 405
38. L. E. Gordon, Nucl. Phys. B **501** (1997) 197

Appendix

Here we present formulae for the subtraction term in the cross section for the production of the isolated photon (see sec. 3) in the $\gamma p \rightarrow \gamma X$ scattering. The corresponding expressions for the ep reaction can be obtained using the equivalent photon approximation (sec. 4). The subtraction term is the cross section for subprocesses in which the energy of hadrons inside the cone of radius R around the final photon is higher than the energy of the photon multiplied by a small parameter ϵ ,

$$\sum_h E_h > \epsilon E_\gamma. \quad (12)$$

The cone is defined in the rapidity and azimuthal angle plane:

$$\sqrt{(\eta_h - \eta_\gamma)^2 + (\phi_h - \phi_\gamma)^2} \leq R. \quad (13)$$

Below we use the variables v and w defined in the following way:

$$v = 1 + \frac{\hat{t}}{\hat{s}}, \quad w = \frac{-\hat{u}}{\hat{s} + \hat{t}},$$

where \hat{s} , \hat{t} and \hat{u} are the Mandelstam variables for the partonic subprocess,

$$\hat{s} = yx_\gamma x S_{ep}, \quad \hat{t} = yx_\gamma z T_{ep}, \quad \hat{u} = xz U_{ep},$$

and S_{ep} , T_{ep} and U_{ep} stand for the Mandelstam variables for $ep \rightarrow e\gamma X$ reaction,

$$S_{ep} = 2p_e p_p, \quad T_{ep} = -2p_e p_\gamma, \quad U_{ep} = -2p_p p_\gamma.$$

The p_e , p_p and p_γ denote the initial electron and proton four-momenta and the four-momentum of the final photon, respectively. The fractional momenta y , x_γ , x and z are defined in secs. 2.2 and 4.

The subtraction cross section consists from two contributions which arise from subprocesses involving fragmentation function and from α_s corrections to the Born process:

$$E_\gamma \frac{d^3 \sigma_{sub}^{\gamma p \rightarrow \gamma X}}{d^3 p_\gamma} = E_\gamma \frac{d^3 \sigma_{frag}^{\gamma p \rightarrow \gamma X}}{d^3 p_\gamma} + E_\gamma \frac{d^3 \sigma_{cor}^{\gamma p \rightarrow \gamma X}}{d^3 p_\gamma}, \quad (14)$$

where

$$\begin{aligned} E_\gamma \frac{d^3 \sigma_{frag}^{\gamma p \rightarrow \gamma X}}{d^3 p_\gamma} &= \sum_{b=g,q,\bar{q}} \sum_{c=g,q,\bar{q}} \int_0^{1/(1+\epsilon)} \frac{dz}{z^2} \int_0^1 dx f_{b/p}(x, \bar{Q}^2) D_{\gamma/c}(z, \bar{Q}^2) E_\gamma \frac{d^3 \sigma^{\gamma b \rightarrow cd}}{d^3 p_\gamma} + \\ &+ \sum_{a=g,q,\bar{q}} \sum_{b=g,q,\bar{q}} \sum_{c=g,q,\bar{q}} \int_0^{1/(1+\epsilon)} \frac{dz}{z^2} \int_0^1 dx_\gamma \int_0^1 dx f_{a/\gamma}(x_\gamma, \bar{Q}^2) f_{b/p}(x, \bar{Q}^2) D_{\gamma/c}(z, \bar{Q}^2) E_\gamma \frac{d^3 \sigma^{ab \rightarrow cd}}{d^3 p_\gamma} \end{aligned} \quad (15)$$

and

$$\begin{aligned} E_\gamma \frac{d^3 \sigma_{cor}^{\gamma p \rightarrow \gamma X}}{d^3 p_\gamma} &= \sum_{i=1}^{2N_f} \int_{x_0}^1 dx \Theta \left(\frac{v(1-w)}{1-v+vw} - \epsilon \right) \cdot \\ &\cdot \left[f_{q_i/p}(x, \bar{Q}^2) E_\gamma \frac{d^3 \sigma_{sub}^{\gamma q_i \rightarrow \gamma q_i + g}}{d^3 p_\gamma} + f_{q_i/p}(x, \bar{Q}^2) E_\gamma \frac{d^3 \sigma_{sub}^{\gamma q_i \rightarrow \gamma g + q_i}}{d^3 p_\gamma} + f_{g/p}(x, \bar{Q}^2) E_\gamma \frac{d^3 \sigma_{sub}^{\gamma g \rightarrow \gamma q_i + \bar{q}_i}}{d^3 p_\gamma} \right] \end{aligned} \quad (16)$$

with

$$x_0 = \frac{-yT_{ep}}{yS_{ep} + U_{ep}}.$$

The contribution (15) comes from $2 \rightarrow 2$ single and double resolved subprocesses in which the final c -parton decays into the photon. Here the calculations are standard, as for non-isolated photon case⁴⁻⁹. The condition (12) is included via the upper limit of the integration over z : $z \equiv E_\gamma/E_c < 1/(1+\epsilon)$ (the hadron remnant of the c -parton takes the energy $E_h = E_c - E_\gamma$, so $E_h = (1/z - 1)E_\gamma > \epsilon E_\gamma$). The lower limit of the integration over the fractional momenta z , x_γ and x is formally zero but in fact this zero-value is inaccessible due to the delta function, $\delta(yx_\gamma xS_{ep} + yx_\gamma zT_{ep} + xzU_{ep})$, in the partonic cross sections for $2 \rightarrow 2$ subprocesses.

The contribution (16) describes the α_s corrections to the Born process. The diagrams involving the virtual gluon exchange do not contribute to the subtraction term, and only $2 \rightarrow 3$ processes are included. In these processes the photon and two partons are produced. One of the partons enters the cone of radius R around the photon, and its energy should be higher than the photon's energy multiplied by ϵ . To fulfill this condition the integration is performed over x values for which $v(1-w)/(1-v+vw) > \epsilon$. There are three types of such processes:

- $\gamma q \rightarrow \gamma q + g$ (with a quark inside the cone),
- $\gamma q \rightarrow \gamma g + q$ (with a gluon inside the cone),
- $\gamma g \rightarrow \gamma q + \bar{q}$ (with a quark inside the cone).

Below we present our analytical results for the α_s corrections contributing to the subtraction term. The results are obtained with the assumption that the angle between the photon and the parton inside the cone is small. The quark masses are neglected. All collinear singularities are shifted into the fragmentation functions $D_{\gamma/c}$ (infrared singularities do not appear in this calculations). The p_T stands for the transverse momentum of the final photon. The partonic cross sections in (16) are given by following expressions:

$$E_\gamma \frac{d^3\sigma_{sub}^{\gamma q_i \rightarrow \gamma q_i + g}}{d^3p_\gamma} = \frac{4}{3} \frac{\alpha_{em}^2 \alpha_s}{\pi \hat{s}^2} e_{q_i}^4 \left[\frac{(1-v+vw)^2 + (1-v)^2}{(1-v+vw)(1-v)} P(\bar{Q}^2) + \frac{(Rp_T)^2}{\hat{s}} \frac{(vw)^3}{(1-v+vw)(1-v)^2} \right], \quad (17)$$

$$E_\gamma \frac{d^3\sigma_{sub}^{\gamma q_i \rightarrow \gamma g + q_i}}{d^3p_\gamma} = \frac{4}{3} \frac{\alpha_{em}^2 \alpha_s}{\pi \hat{s}^2} e_{q_i}^4 \frac{(Rp_T)^2}{\hat{s}} \frac{(1-v)[(1-v+vw)^2 + (vw)^2]}{(1-v+vw)^5 v(1-w)(vw)^2} [1 + (1-v+vw)^4 + v^4(1-w)^4], \quad (18)$$

$$E_\gamma \frac{d^3\sigma_{sub}^{\gamma g \rightarrow \gamma q_i + \bar{q}_i}}{d^3p_\gamma} = \frac{1}{2} \frac{\alpha_{em}^2 \alpha_s}{\pi \hat{s}^2} e_{q_i}^4 \left[\frac{(vw)^2 + (1-v)^2}{vw(1-v)} P(\bar{Q}^2) + \frac{(Rp_T)^2}{\hat{s}} \frac{(1-v+vw)^4}{(vw)^2(1-v)^2} \right], \quad (19)$$

where

$$P(\bar{Q}^2) = \frac{1+v^2(1-w)^2}{(1-v+vw)^2} \ln \left(\frac{R^2 p_T^2 v^2 (1-w)^2}{\bar{Q}^2} \right) + 1. \quad (20)$$

Table 1: The cross section for non-isolated and isolated final photon, isolated photon with $0.2 \leq y \leq 0.9$, and isolated photon with $0.2 \leq y \leq 0.9$ and $-0.7 \leq \eta^\gamma \leq 0.9$.

[pb]	total	Born	$O(\alpha_S)$	box	single resolved initial γ	single resolved final γ	double resolved
non-isolated	226.2	82.1 (36.3%)	8.7 (3.8%)	13.9 (6.1%)	54.7 (24.2%)	24.6 (10.9%)	42.2 (18.7%)
isolated	180.4	82.1 (45.5%)	15.2 (8.4%)	13.9 (7.7%)	54.7 (30.3%)	5.12 (2.8%)	9.37 (5.2%)
isolated y cut	72.33	23.6 (32.6%)	6.33 (8.8%)	6.54 (9.0%)	28.2 (39.0%)	2.34 (3.2%)	5.29 (7.3%)
isolated y, η_γ cuts	35.36	13.6 (38.5%)	3.32 (9.4%)	3.41 (9.6%)	11.9 (33.7%)	1.21 (3.4%)	1.92 (5.4%)

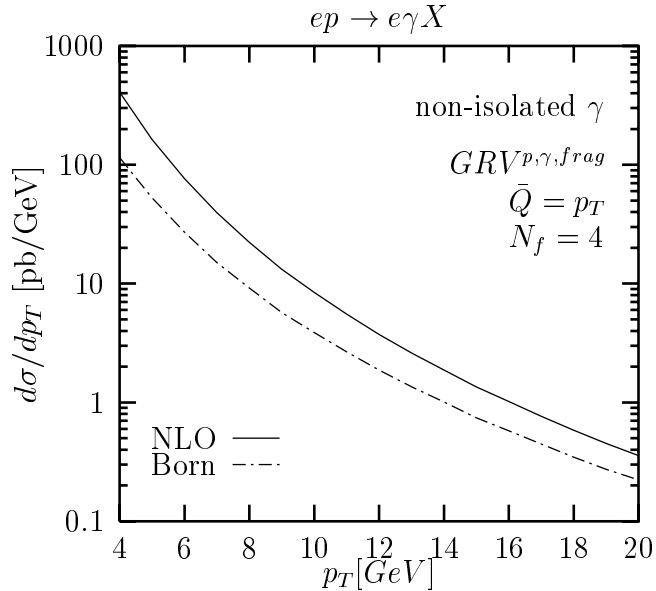


Figure 6: The final photon p_T -dependence of the cross section $d\sigma/dp_T$ for non-isolated γ photoproduction (solid line). The Born contribution is shown separately (dash-dotted line).

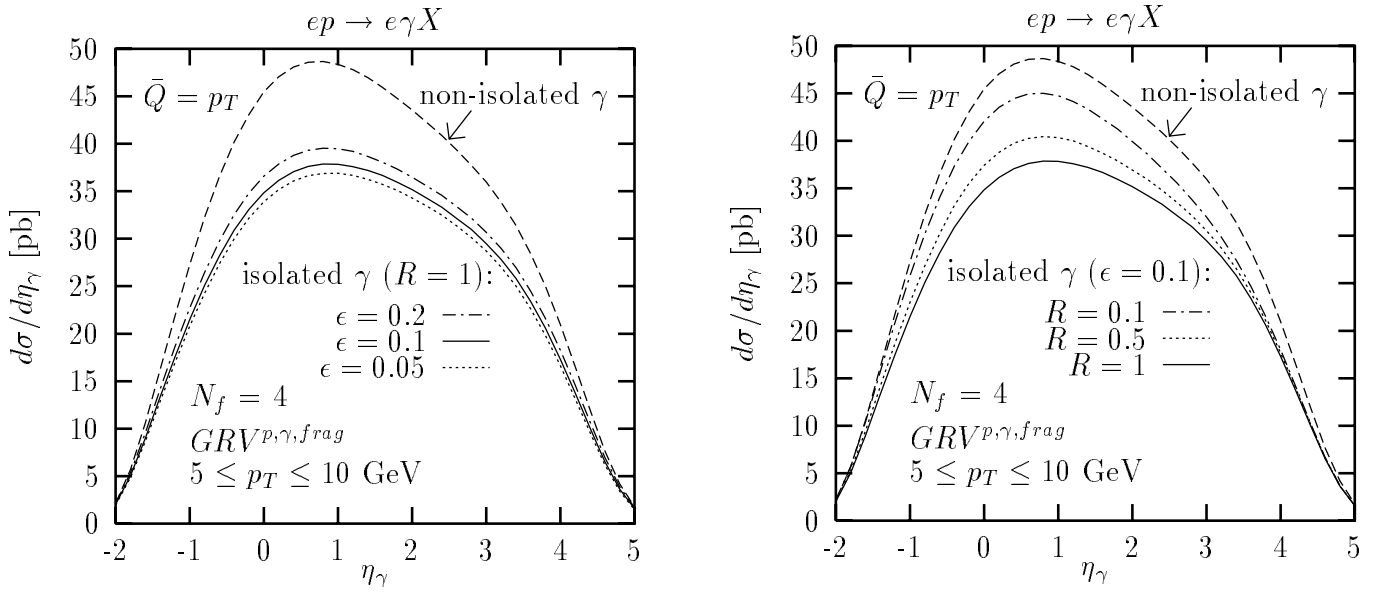


Figure 7: The differential cross section $d\sigma/d\eta_\gamma$ as a function of the photon rapidity η_γ . a) The results for non-isolated photon (dashed line) and isolated photon with $R = 1$ and $\epsilon = 0.05$ (dotted line), 0.1 (solid line) and 0.2 (dot-dashed line). b) The results for non-isolated photon (dashed line) and isolated photon with $\epsilon = 0.1$ and $R = 0.1$ (dot-dashed line), 0.5 (dotted line) and 1 (solid line).

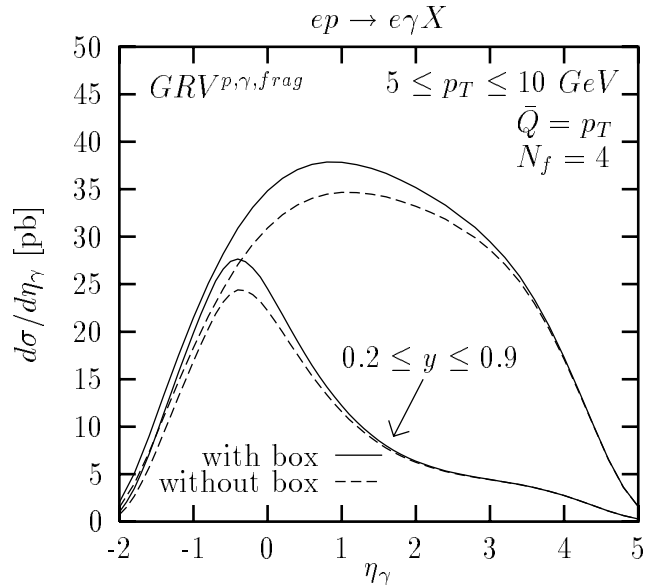


Figure 8: The differential cross section $d\sigma/d\eta_\gamma$ for isolated γ ($\epsilon = 0.1$, $R = 1$) as a function of the photon rapidity η_γ with (solid lines) and without (dashed lines) the box contribution. The results are obtained with imposed y cut ($0.2 \leq y \leq 0.9$) and without this cut.

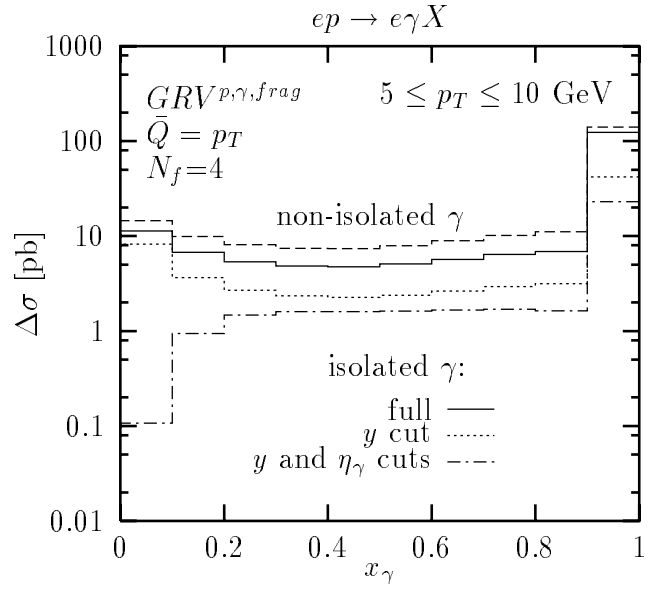


Figure 9: The cross section in x_γ bins of the length 0.1. The results for non-isolated γ integrated over the whole range of y and η_γ are shown with the dashed line. The solid line represents results integrated over the whole range of y and η_γ for isolated γ with $\epsilon = 0.1$ and $R = 1$. Results with additional cuts in the isolated γ cross section are shown with: dotted line ($0.2 \leq y \leq 0.9$) and dot-dashed line ($0.2 \leq y \leq 0.9$, $-0.7 \leq \eta_\gamma \leq 0.9$).

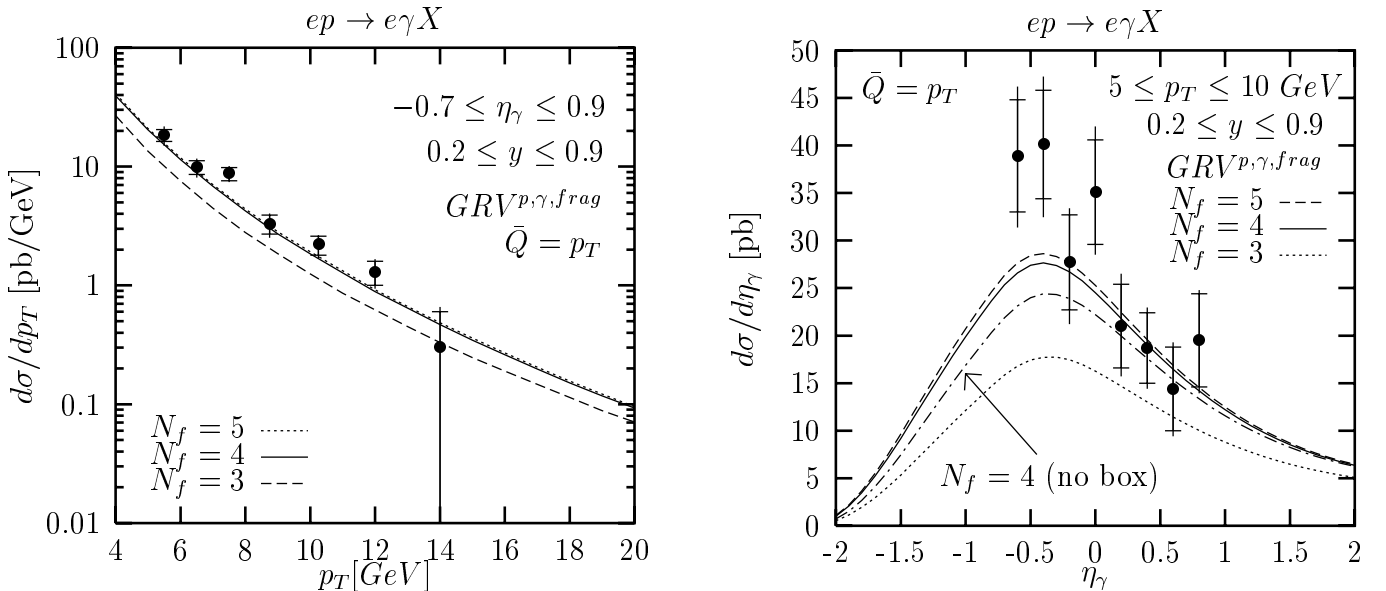


Figure 10: The results for isolated γ with various numbers of active massless flavors: $N_f = 3$ (dashed lines), 4 (solid lines) and 5 (dotted lines), compared to the ZEUS data¹². a) The differential cross section $d\sigma/dp_T$ as a function of the photon transverse momentum. b) The differential cross section $d\sigma/d\eta_\gamma$ as a function of the photon rapidity η_γ ; the result without the box contribution is also shown for $N_f = 4$ (dot-dashed line).

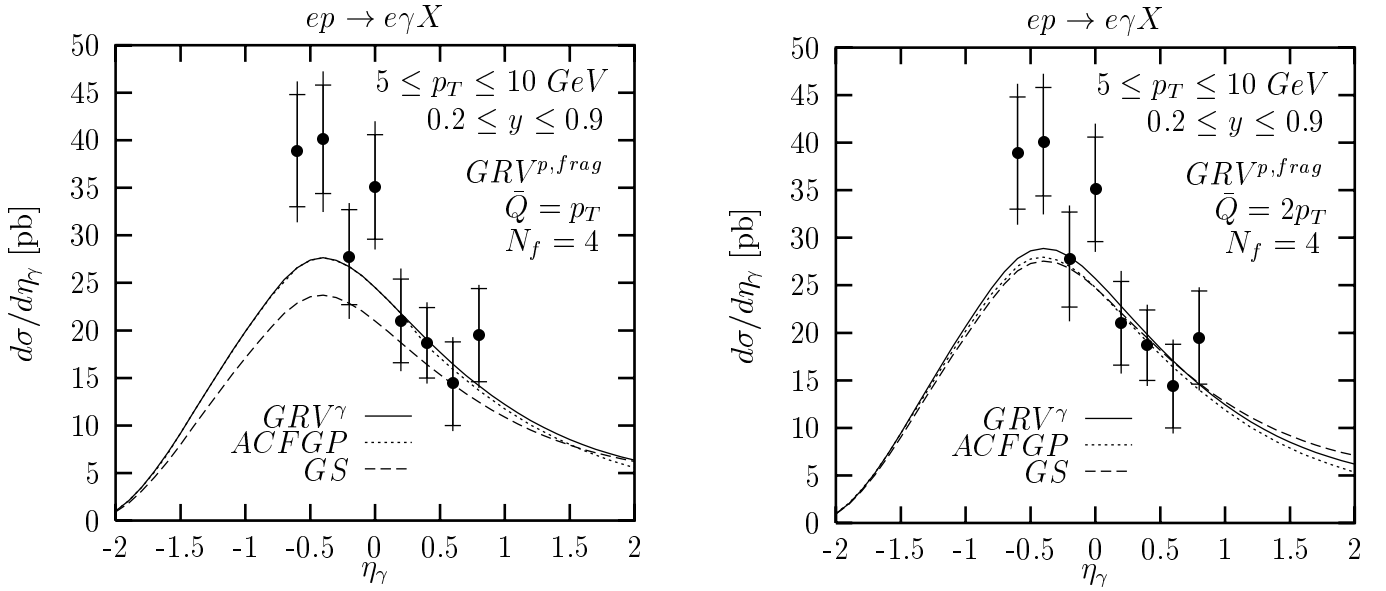


Figure 11: The differential cross section $d\sigma/d\eta_\gamma$ for isolated γ as a function of the photon rapidity η_γ compared to the ZEUS data¹². Three different NLO photon parton distributions are used: ACFGp⁸ (dotted line), GRV³³ (solid line) and GS³⁷ (dashed line). The GRV NLO parton distributions in the proton³² and parton fragmentation into photon³⁴ are used. a) $\bar{Q} = p_T$. b) $\bar{Q} = 2p_T$.

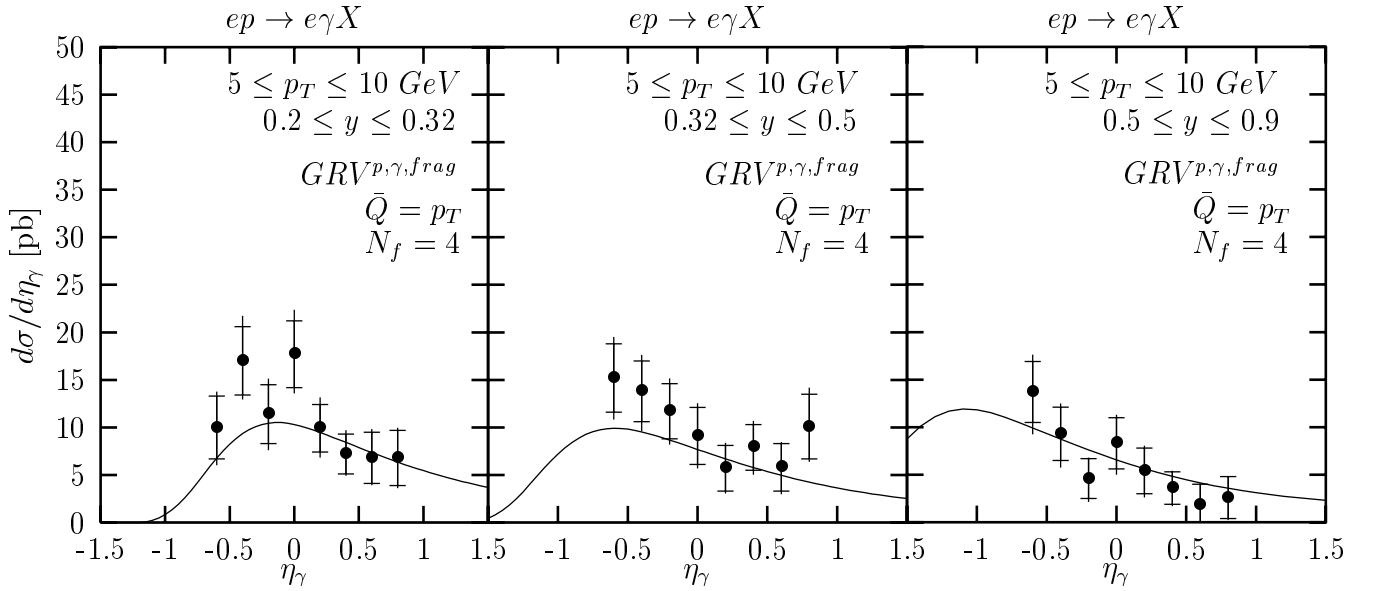


Figure 12: The results for three ranges of y : $0.2 < y < 0.32$, $0.32 < y < 0.5$ and $0.5 < y < 0.9$, compared to the ZEUS data¹².

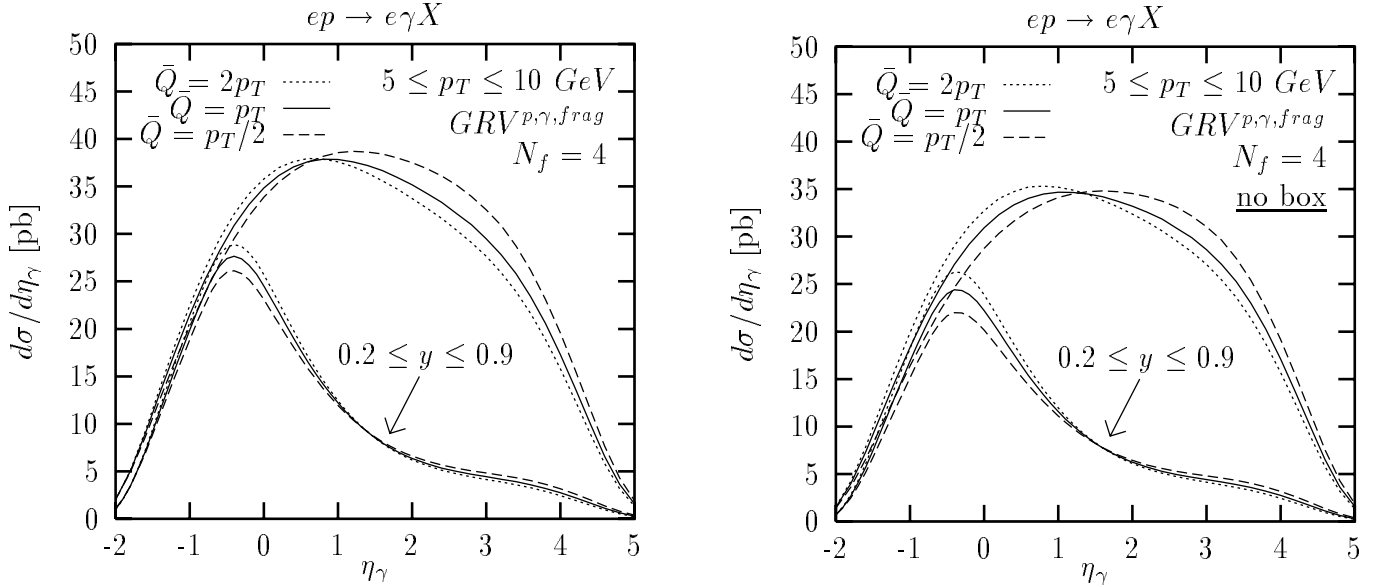


Figure 13: The differential cross section $d\sigma/d\eta_\gamma$ for isolated γ photoproduction as a function of the photon rapidity η_γ with (a) and without (b) the box contribution. Three different values of the \bar{Q} scale are assumed: $\bar{Q} = p_T/2$ (dashed lines), $\bar{Q} = p_T$ (solid lines) and $\bar{Q} = 2p_T$ (dotted lines). The results are obtained with imposed y cut ($0.2 \leq y \leq 0.9$) and without this cut.

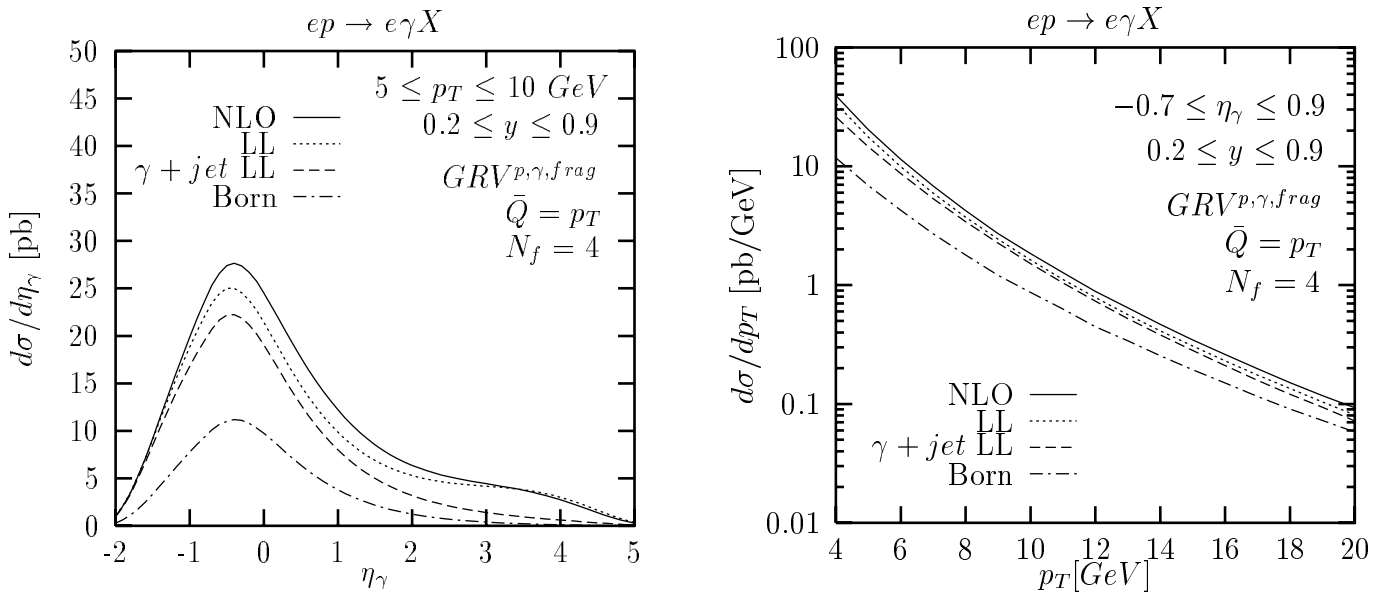


Figure 14: The differential cross sections $d\sigma/d\eta_\gamma$ (a) and $d\sigma/dp_T$ (b): NLO (solid line) and LL (dotted line) results for isolated γ , and LL predictions for isolated $\gamma + \text{jet}$ photoproduction (dashed line); the jet rapidity is assumed in the range: $-1.5 \leq \eta_{\text{jet}} \leq 1.8$. The dot-dashed lines show the Born contribution to the NLO cross section for isolated γ . GRV NLO (LO) parton densities in the proton and photon were applied in NLO (LL) calculations.